

Electronic level structure of Th^+ in the range of the ^{229m}Th isomer energy

D.-M. Meier,¹ J. Thielking,¹ P. Głowacki,^{1,*} M. V. Okhapkin,¹ R. A. Müller,¹ A. Surzhykov,^{1,2} and E. Peik^{1,†}

¹Physikalisch-Technische Bundesanstalt, 38116 Braunschweig, Germany

²Technische Universität Braunschweig, 38106 Braunschweig, Germany

(Dated: May 16, 2019)

Using resonant two-step laser excitation of trapped $^{232}\text{Th}^+$ ions, we observe 166 previously unknown energy levels of even parity within the energy range from 7.8 to 9.8 eV and angular momenta from $J = 1/2$ to $7/2$. We also classify the high-lying levels observed in our earlier experiments by the total angular momentum and perform multiconfiguration Dirac-Fock (MCDF) calculations to compare their results with the observed level density. The observed levels can be relevant for the excitation or decay of the ^{229m}Th isomeric nuclear state which lies in this energy range. The high density of electronic levels promises a strongly enhanced electronic bridge excitation of the isomer in $^{229}\text{Th}^+$.

PACS numbers: 42.62.Fi, 32.30.-r

Keywords: laser spectroscopy, atomic structure, thorium

I. INTRODUCTION

The atomic structure of thorium, the third-heaviest naturally occurring element, has been a subject of study because of applications in various fields. With four valence electrons in neutral Th and strongly mixed 5f, 6d, 7s and 7p configurations the atomic spectrum is dense and complex [1]. The high density of lines makes thorium discharge lamps suitable for the calibration of spectrographs over wide spectral ranges, for example in astronomical observatories [2, 3]. In a recent analysis of the spectra of Th, Th^+ and Th^{2+} , Ritz wavelengths of about 20000 lines are given together with 787 energy levels of Th and 516 of Th^+ [3].

In our earlier work [4] on Th^+ we have seen the onset of repulsion in the energy spacing between levels of identical parity and angular momentum, as it is expected for strong configuration mixing, leading to the appearance of chaotic quantum dynamics [5].

Work on excited states in Th^+ is motivated by the search for laser excitation of the ^{229m}Th nuclear isomer at 7.8 eV excitation energy. This energy has been inferred from γ -spectroscopy [6, 7] with an uncertainty $\sigma = 0.5$ eV, that is large on the scale of optical spectroscopy. No direct optical spectroscopy of the nuclear transition has been possible so far. Since the electronic level density in this energy range is high, it can be expected that laser excitation of the isomer and radiative decay are dominated by so called electronic bridge processes, where the electron shell enhances the coupling of the nucleus to the radiation field [8–11], determined by the detuning between nuclear and electronic resonance. Therefore it is likely to find strong enhancement in a system with high electronic level density. A tentative experimental indication of this mechanism could be conjectured from the observation of a strongly reduced lifetime of the isomer in Th^+ in comparison to Th^{2+} and Th^{3+} [12, 13].

In a previous publication [4] 44 unknown energy levels of Th^+ were reported within the energy range from 7.3 to 8.3 eV, obtained from two-step laser excitation of trapped Th^+ ions. Extending this study, we present here

166 additional levels of even parity up to 9.8 eV energy and classify these and the levels reported earlier according to their total angular momentum. In order to excite different configurations and different values of the angular momentum, 15 different intermediate levels are used as first excitation steps from the ground state. Figure 1 gives a schematic overview of the excitation schemes and Table I lists the leading electronic configurations of the intermediate levels used in our experiments.

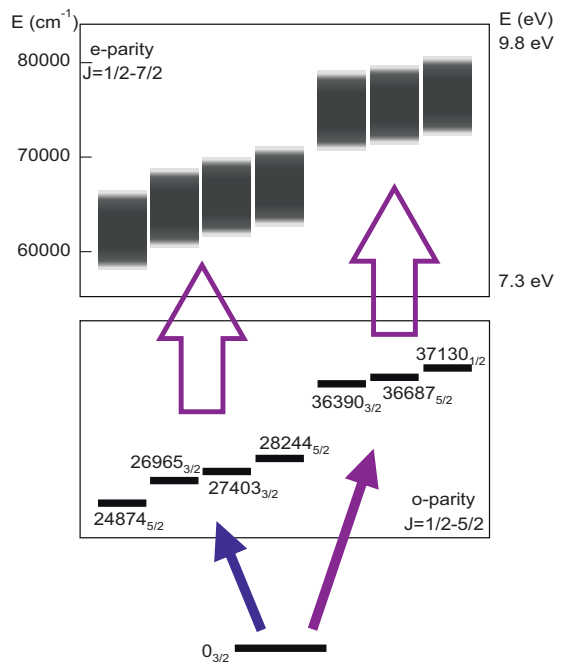


FIG. 1. Two-step laser excitation scheme in Th^+ , starting from the ground state through different odd-parity intermediate levels (middle panel) to high-lying levels within the indicated energy ranges (upper panel). Levels are labelled by their energy in cm^{-1} and their total angular momentum J .

The range of excitation energy that is investigated here covers more than 2σ above the ^{229m}Th isomer energy of 7.8(5) eV, but is still well below the ionization potential of Th^+ of 12.1(2) eV [4]. A further increase in level density by up to a factor ten has been predicted in approaching the ionization energy [16]. Multi-configurational Dirac-Fock (MCDF) calculations are used to estimate the level density in the range of the excitation energy of the nuclear

* Present address: Poznań University of Technology, Poznań, Poland

† Corresponding author e-mail address: ekkehard.peik@ptb.de

TABLE I. Intermediate levels of the two-step excitation, sorted by angular momentum J . Energies and leading configurations are taken from Ref. [14], with the exception of the corrected classification of the 25027cm^{-1} state described in Ref. [15]. Labels in the first column are introduced for reference in Tab. III in the appendix.

Ref.	Level [cm $^{-1}$]	J	Configuration
a	25027.040	1/2	$7s7p + 6d7s7p$
b	26626.478	1/2	$6d7s(^3D)7p\ ^4D^o + (^3D)\ ^2P^o$
c	35198.990	1/2	$6d^2(^3P)7p\ ^4D^o + 6d7s(^3D)7p\ ^4P^o$
d	37130.340	1/2	$5f(^1G^o)6d^2\ ^2P^o + 6d^2(^3P)7p\ ^4D^o$
e	37716.322	1/2	$6d^2(^1D)7p\ ^2P^o + (^3F)\ ^4D^o$
f	26965.202	3/2	$5f(^3F^o)6d^2\ ^4S^o + (^3F^o)\ ^2P^o$
g	27403.180	3/2	$5f(^1D^o)6d^2\ ^2D^o + (^3P^o)\ ^4D^o$
h	36390.527	3/2	$6d^2(^3F)7p\ ^4F^o + 5f(^1G^o)6d^2\ ^2P^o$
i	36581.568	3/2	$6d^2(^3F)7p\ ^4F^o + 5f(^1G^o)6d^2\ ^2D^o$
j	24873.981	5/2	$6d7s(^3D)7p\ ^4F^o + 5f(^3P^o)6d^2\ ^4F^o$
k	26424.480	5/2	$5f(^3P^o)6d^2\ ^4F^o + (^3P^o)\ ^4D^o$
l	28243.812	5/2	$6d7s(^3D)7p\ ^4F^o + 6d^2(^3F)7p\ ^4G^o$
m	35156.916	5/2	$5f(^1G^o)6d^2\ ^2D^o + (^1G^o)\ ^2F^o$
n	36687.992	5/2	$6d^2(^3F)7p\ ^4F^o + 6d7s(^3D)7p\ ^4P^o$
o	37846.174	5/2	$6d^2(^3P)7p\ ^2D^o + (^3P)\ ^4D^o$

isomer.

II. EXPERIMENTAL

For the experiments we use a linear Paul trap with the capacity to store up to 10^6 $^{232}\text{Th}^+$ ions, described in Ref. [17, 18]. The trap is loaded by ablating a metallic ^{232}Th target using a Nd:YAG laser emitting 5 ns pulses with an energy of $\leq 1\text{ mJ}$ at 1064 nm. Argon buffer gas at 0.1 Pa pressure is used to cool the trapped ions to room temperature and to depopulate metastable states by collisional quenching [17, 18]. We dissociate Th^+ molecular compounds which are formed in the trap with impurities of the buffer gas (see [4]) with the 4th harmonic radiation of a Q-switched solid state laser at 266 nm and a pulse energy of $\approx 10\mu\text{J}$.

The search of new levels is carried out by a two-step excitation: An odd-parity intermediate level (see Tab. I) is excited from the ground state and the radiation frequency of a second laser is tuned over a wide frequency range to excite unknown even-parity high-lying levels from the intermediate level. A scheme of the experimental setup is shown in Fig. 2. The first excitation step is provided by the radiation of a second harmonic (SHG) or third harmonic generation (THG) of a pulsed Ti:Sa laser (TU model, Photonics Industries). For the second excitation step we use the radiation of a THG of a second pulsed Ti:Sa laser (Credo, Sirah Lasertechnik).

Both lasers emit synchronized pulses with a duration of $\approx 20\text{ ns}$ and a repetition rate of 1 kHz. The beam diameters of both lasers, which are matched at the position of the ions in the linear Paul trap, are $\approx 1\text{ mm}$ and the peak powers used in the experiment are up to 0.1 kW, which corresponds to intensities of 10 kW/cm^2 . The wavelengths of both lasers are measured by a Fizeau-wavemeter (HighFinesse/Angstrom WS-7). The first laser wavelength is stabilized to the center of the Doppler-broadened line of one of a set of selected intermediate levels by a computer-based locking scheme using the

wavemeter readout. The second laser is tunable by controlling an intracavity diffraction grating and simultaneously adjusting the orientation of the frequency conversion crystals. The third harmonic radiation is tuned in the range from 240 to 293 nm at a tuning rate of 0.001 nm/s in frequency steps of $\approx 500\text{ MHz}$ (0.1 pm) or $\approx 100\text{ MHz}$ for fine scans. In the search for new levels we determine the line center of each transition by repeated fine scanning over the line.

For the detection of the fluorescence decay of the high-lying electronic levels we use two photomultiplier tubes (PMT) for different spectral ranges. Photons are detected in the range from 300 to 650 nm with a PMT which is equipped with a long-pass edge interference filter to block laser stray light from the Ti:Sa laser pulses. A second PMT is used for the detection of VUV photons in the wavelength range from 115 to 230 nm. Fast gated integrators are used to evaluate the PMT signals during a detection window of 100 ns, starting after the excitation pulses. Counters are used to detect photons in the interval from 1 to 10 μs after the excitation pulses.

We try to excite each observed level via several intermediate levels with different values of the angular momentum (see Tab. 1) to confirm them as high-lying levels and determine their total angular momenta.

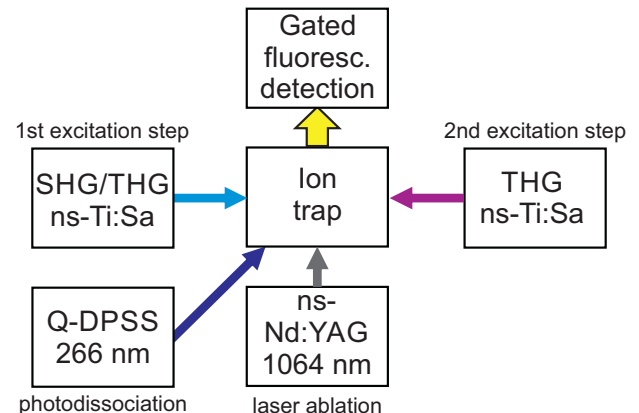


FIG. 2. Experimental setup for laser excitation of trapped Th^+ ions. The first step excitation is provided by the second harmonic (SHG) or third harmonic (THG) radiation of a nanosecond Ti:Sa laser, locked to a Fizeau wavemeter. The second excitation step is provided by the THG of a second ns-Ti:Sa laser. Th^+ ions are loaded via laser ablation (ns-Nd:YAG laser at 1064 nm). Molecular compounds of Th^+ are photodissociated by pulses from a Q-switched diode-pumped solid-state laser (Q-DPSS) at 266 nm.

III. NEWLY OBSERVED LEVELS

Within the search scans we not only observe direct two-step excitation to high-lying levels, but also single-photon transitions originating from the ground state, thermally populated metastable levels (up to 4490 cm^{-1}) and levels populated by a decay of the intermediate level (N-scheme transition). Most of these transitions can be identified based on the existing energy level database [14]. In order to unambiguously identify new levels at an excitation energy corresponding to the sum of the two laser photon energies, we require to observe the excitation via at least

two intermediate levels.

Excitation of a high-lying level is inferred by observing either fluorescence at a wavelength different from the excitation wavelength, depletion of fluorescence from the decay of the intermediate level or a loss of ions because of resonance-enhanced three-photon ionization, see Fig. 3. Due to the high pulse power of the Ti:Sa laser radiation there is a significant probability of absorption of a third photon when a high-lying level is excited. The absorp-

tion of this photon leads to ionization of the Th^+ ions to Th^{2+} ions [4]. We select the operating parameters of our ion trap so that Th^{2+} is not stably trapped. Nevertheless, ionization alone cannot be a confirmation of the high-lying level excitation, because it can also occur as a resonant four-photon process in an N-scheme excitation through levels with an energy of about 20000 cm^{-1} , listed in Ref. [14].

TABLE II: Newly found electronic levels in $^{232}\text{Th}^+$ in the energy range from 7.8 to 9.8 eV, total uncertainties σ_{tot} of the energy determination and possible angular momenta. The angular momentum value $J = 3/2$ is assigned with certainty, otherwise the most likely values of J are given (see text). Levels marked with * were found in the previous investigation [4] with an uncertainty of 0.2 cm^{-1} and are classified in this investigation. We update the energy value of a previously found level, marked with **.

Energy [cm^{-1}]	σ_{tot} [cm^{-1}]	J	Energy [cm^{-1}]	σ_{tot} [cm^{-1}]	J	Energy [cm^{-1}]	σ_{tot} [cm^{-1}]	J
58875.5	*	3/2 - 7/2	68564.19	0.18	3/2 or 5/2	74195.13	0.17	3/2 - 7/2
59387.1	*	3/2 - 7/2	68598.83	0.18	3/2 or 5/2	74201.68	0.16	1/2 or 3/2
59477.4	*	3/2	68752.06	0.17	3/2	74255.11	0.17	3/2 or 5/2
59803.0	*	3/2 - 7/2	68812.64	0.18	3/2 or 5/2	74328.90	0.17	3/2 or 5/2
60380.1	*	3/2	68898.67	0.17	3/2 or 5/2	74396.40	0.16	3/2 or 5/2
60618.6	*	3/2	68921.30	0.17	3/2 or 5/2	74461.06	0.17	3/2 - 7/2
60721.3	*	3/2 - 7/2	69582.93	0.17	3/2	74503.38	0.18	3/2 or 5/2
61032.4	*	3/2	70036.57	0.17	3/2	74554.39	0.16	3/2
61388.0	*	3/2 - 7/2	70602.32	0.16	3/2 or 5/2	74642.51	0.17	3/2 or 5/2
61428.6	*	3/2 or 5/2	70618.40	0.16	3/2 or 5/2	74646.94	0.16	1/2 or 3/2
61726.3	*	3/2	70747.82	0.16	3/2 - 7/2	74781.76	0.17	3/2 or 5/2
61963.6	*	3/2	70924.75	0.16	3/2 or 5/2	74823.59	0.16	3/2 or 5/2
62307.2	*	3/2 or 5/2	71038.37	0.16	3/2	74881.76	0.17	3/2
62373.8	*	3/2	71043.67	0.15	3/2 - 7/2	75009.01	0.18	3/2 or 5/2
62477.0	*	3/2 or 5/2	71148.96	0.16	3/2 or 5/2	75058.06	0.17	3/2 - 7/2
62560.1	*	3/2 or 5/2	71153.87	0.16	3/2	75108.36	0.17	3/2 or 5/2
62562.2	*	3/2	71278.32	0.16	1/2 or 3/2	75129.42	0.17	1/2 - 5/2
62753.1	*	3/2 or 5/2	71309.24	0.16	3/2 or 5/2	75172.74	0.19	3/2 or 5/2
62873.11	0.17	1/2 or 3/2	71345.59	0.16	1/2 or 3/2	75324.44	0.17	3/2 - 7/2
63257.5	*	3/2 - 7/2	71457.82	0.16	3/2 - 7/2	75380.56	0.17	3/2 or 5/2
63268.90	0.17	1/2 or 3/2	71543.05	0.16	3/2	75434.83	0.17	3/2 - 7/2
63298.4	*	3/2 - 7/2	71544.12	0.16	1/2 or 3/2	75553.70	0.17	1/2 or 3/2
63557.7	*	3/2 - 7/2	71595.39	0.17	1/2 - 5/2	75568.80	0.17	3/2 or 5/2
63680.29	0.16	3/2	71648.63	0.16	1/2 - 5/2	75613.54	0.17	3/2
64107.51	0.17	3/2 or 5/2	71682.08	0.16	1/2 or 3/2	75690.72	0.17	1/2 or 3/2
64122.0	*	3/2 - 7/2	71704.43	0.16	3/2 or 5/2	75783.69	0.17	3/2 or 5/2
64150.3	*	3/2	71893.76	0.16	3/2	75840.96	0.16	3/2 or 5/2
64368.24	0.17	3/2 or 5/2	71980.22	0.17	3/2 or 5/2	75889.36	0.17	1/2 or 3/2
64442.11	0.16	1/2 or 3/2	71995.47	0.16	3/2 - 7/2	75950.56	0.17	3/2 - 7/2
64560.4	*	3/2	72027.87	0.16	3/2	75966.37	0.16	3/2
64813.7	*	3/2 - 7/2	72070.57	0.16	1/2 or 3/2	76122.62	0.16	1/2 or 3/2
64860.4	*	3/2 or 5/2	72183.47	0.17	3/2 or 5/2	76157.73	0.16	1/2 or 3/2
64887.80	0.16	1/2 or 3/2	72195.77	0.17	3/2 or 5/2	76158.83	0.17	3/2 - 7/2
64920.1	*	3/2 or 5/2	72353.67	0.17	3/2 - 7/2	76169.30	0.17	1/2 - 5/2
65037.7	*	3/2	72395.99	0.18	3/2 or 5/2	76227.32	0.17	1/2 - 5/2
65144.4	*	3/2 or 5/2	72403.45	0.16	3/2	76371.41	0.16	1/2 or 3/2
65191.1	*	3/2 - 7/2	72437.78	0.16	1/2 or 3/2	76445.96	0.16	1/2 or 3/2
65730.4	*	3/2	72443.68	0.16	3/2 or 5/2	76508.84	0.17	3/2 - 7/2
65738.54	0.18**	3/2 - 7/2	72612.99	0.18	3/2 or 5/2	76521.57	0.17	3/2 or 5/2
65753.45	0.17	1/2 or 3/2	72624.83	0.16	3/2	76552.60	0.16	3/2
65799.6	*	3/2	72644.97	0.16	3/2 - 7/2	76616.44	0.17	3/2 - 7/2
65910.0	*	3/2 - 7/2	72711.86	0.16	3/2 - 7/2	76788.94	0.16	1/2 or 3/2
65946.9	*	3/2 - 7/2	72748.31	0.16	3/2	76895.40	0.16	3/2
66052.0	*	3/2 or 5/2	72756.38	0.17	3/2 - 7/2	76954.26	0.16	3/2
66141.2	*	3/2 or 5/2	72849.84	0.16	3/2	76999.66	0.16	3/2 - 7/2
66324.52	0.17	1/2 or 3/2	72904.32	0.16	3/2 - 7/2	77069.42	0.17	3/2 or 5/2
66333.7	*	3/2	72937.01	0.17	3/2 or 5/2	77154.88	0.17	1/2 - 5/2
66388.81	0.17	1/2 or 3/2	72967.30	0.16	3/2	77185.31	0.16	3/2 - 7/2
66429.64	0.17	3/2 or 5/2	73007.80	0.16	1/2 or 3/2	77208.86	0.17	3/2 or 5/2

TABLE II: Cont.: Newly found electronic levels in $^{232}\text{Th}^+$.

Energy [cm $^{-1}$]	σ_{tot} [cm $^{-1}$]	J	Energy [cm $^{-1}$]	σ_{tot} [cm $^{-1}$]	J	Energy [cm $^{-1}$]	σ_{tot} [cm $^{-1}$]	J
66558.0	*	3/2 - 7/2	73141.86	0.16	3/2	77278.24	0.16	1/2 or 3/2
66609.0	*	3/2 or 5/2	73171.82	0.17	3/2 - 7/2	77295.28	0.17	3/2 or 5/2
66666.96	0.17	1/2 or 3/2	73225.52	0.17	3/2	77311.25	0.16	3/2
66702.9	*	3/2	73245.52	0.17	3/2 or 5/2	77429.20	0.16	1/2 or 3/2
66831.1	*	3/2	73314.63	0.16	3/2 - 7/2	77506.72	0.16	1/2 - 5/2
66855.6	*	3/2 or 5/2	73349.33	0.18	1/2 or 3/2	77668.89	0.17	3/2 or 5/2
67066.2	*	3/2 - 7/2	73427.59	0.16	3/2	77715.95	0.17	1/2 or 3/2
67154.05	0.16	3/2	73486.18	0.18	3/2 or 5/2	77914.52	0.16	1/2 or 3/2
67177.76	0.18	3/2 - 7/2	73506.20	0.16	1/2 or 3/2	77992.06	0.16	3/2 - 7/2
67378.61	0.19	3/2 - 7/2	73514.42	0.17	3/2 - 7/2	78004.65	0.16	3/2
67509.63	0.17	3/2	73571.40	0.17	3/2 or 5/2	78079.15	0.16	3/2 or 5/2
67577.71	0.20	3/2 or 5/2	73637.54	0.16	3/2 or 5/2	78106.22	0.16	1/2 or 3/2
67657.30	0.18	1/2 or 3/2	73717.33	0.16	3/2	78147.89	0.17	3/2 - 7/2
67737.62	0.18	3/2 or 5/2	73720.66	0.19	3/2 - 7/2	78311.97	0.17	1/2 or 3/2
67803.24	0.17	3/2 or 5/2	73856.76	0.16	3/2 or 5/2	78365.42	0.17	3/2
67843.31	0.17	3/2 or 5/2	73927.39	0.17	3/2 or 5/2	78486.07	0.17	1/2 or 3/2
67866.10	0.18	3/2 or 5/2	74015.17	0.17	3/2 - 7/2	78643.42	0.17	1/2 or 3/2
68033.33	0.21	3/2 - 7/2	74035.55	0.16	3/2	78671.36	0.16	1/2 or 3/2
68088.03	0.17	3/2	74041.31	0.16	3/2 - 7/2	78746.08	0.16	1/2 or 3/2
68278.65	0.20	3/2 - 7/2	74077.59	0.17	1/2 - 5/2	78780.27	0.17	1/2 or 3/2
68497.88	0.18	3/2 or 5/2	74159.76	0.17	3/2 or 5/2	79056.55	0.17	1/2 or 3/2

By applying the aforementioned criteria, two-photon excitations to 166 previously unknown high-lying energy levels in the investigated energy range from 7.3 to 9.8 eV are identified and listed in Tab. II. In Tab. III given in the appendix a complete list with the successful excitation pathways via the different intermediate levels is provided. We achieve a total uncertainty for the energy determination of $\sigma_{tot} \sim 0.2$ cm $^{-1}$, limited by the uncertainty of identifying the center of the Ti:Sa laser spectrum from the wavemeter readout. The energy of a high-lying level is derived as the mean value from the different excitation pathways, weighted with the statistical uncertainty of the individual measurements. The measured center wavelengths of the transitions from the ground state to the intermediate levels mentioned in Tab. I are in coincidence with the values given in Ref. [14].

In comparison to the previous experiment [4] we see an agreement of the measured energies of these levels, except for one level. The energy of the level marked with ** in Tab. II is measured to be 65738.54 cm $^{-1}$, shifted by $\approx 2\sigma$ from the previous value. We verified the existence of the level and update its energy to the new value, which is based on the excitations from three intermediate levels. A level mentioned at 66427.14 cm $^{-1}$ in Ref. [3] is not observed in our experiment.

IV. DETERMINATION OF THE TOTAL ANGULAR MOMENTA

The observed signal strengths at the applied second step laser intensities in the range of 10 kW/cm 2 are in the range expected for electric dipole transitions [4]. Therefore, we assume that the observed transitions are electric dipole allowed. Selection rules then require this high-lying levels to have even parity and angular momenta from $J = 1/2$ to $7/2$, since we are using intermediate levels with $J = 1/2$ to $5/2$.

Analyzing the excitation through different intermediate levels allows for the determination of the total angular momentum of the newly found levels. In our experiment

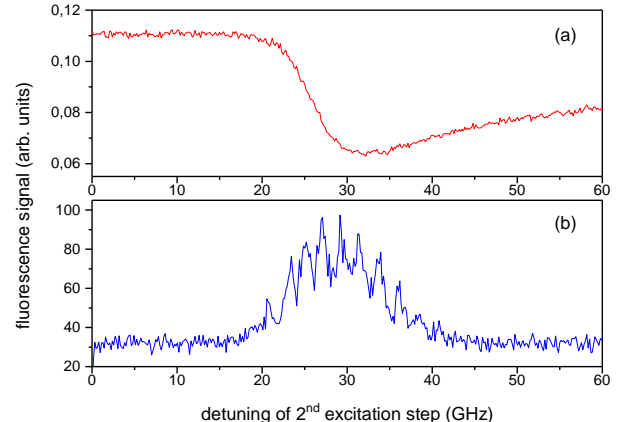


FIG. 3. Two-step excitation of the level 74195.13 cm $^{-1}$ via the intermediate level 35156.9 $_{1/2}$ cm $^{-1}$. Graph (a) shows the decrease of the fluorescence signal of the intermediate level (wavelength range from 325 to 650 nm) due to three-photon ionization during the scan from negative to positive detunings. The slight increase of the signal after the excitation occurs due to redistribution of Th $^+$ ions in the trap. Graph (b) shows the simultaneously recorded VUV fluorescence signal of the decay of the high-lying level. The lineshape is determined by the multimode spectrum of the Ti:Sa laser radiation. The start of the scan at 0 GHz laser detuning corresponds to the wavenumber 39039.15 cm $^{-1}$ of the 2nd excitation step laser radiation.

high-lying levels with $J = 3/2$ can be accessed via all intermediate levels. These states can therefore be unambiguously classified. Angular momenta $J = 1/2, 5/2$ and $7/2$ can only be identified by the absence of excitation through intermediate levels that would not fulfil the $\Delta J = 0, \pm 1$ selection rule.

In these cases, the absence of a single excitation path does not allow a sure assignment of the J value, as we observe that some high-lying levels can be excited through only one out of two intermediate levels with the same J (see, e.g. level 67577.7 cm $^{-1}$, in Tab. III in the appendix).

This is because intermediate levels with the same total angular momenta can have different electronic configurations (see Tab. I) and therefore the excitation probabilities of the high-lying levels can be substantially different. Hence, we require the absence of excitation through at least two intermediate levels with the same J to consider the level not being excitable via this particular J . In all other cases we give the range of possible angular momenta.

Using the same excitation scheme we also determine the angular momenta of levels which could not be classified in Ref. [4].

V. LEVEL DENSITY CALCULATIONS

To reassure that we did not miss a relevant number of levels in the experiment we calculated the densities of even levels in Th^+ up to 85000 cm^{-1} using the multi-configuration Dirac-Fock (MCDF) method implemented in a modified version of the GRASP2K package [19]. A detailed description of the methods involved can be found e.g. in Refs. [20, 21]. Thorium in its singly ionized state has three valence electrons above a closed radon core. The basis for our calculations has been set up with single and double excitations of the valence electrons from six reference configurations: $6d^27s$, $5f^27s$, $5f^26d$, $5f7s7p$, $5f6d7p$ and $6d^3$. Moreover we add to the basis the configurations produced by single excitations from the core opened up to xenon.

Singly charged thorium is a very complicated system with strong electron-electron correlations. Therefore we cannot expect to reproduce the energies of particular levels accurately, especially for high-lying levels. Instead we compare the number of levels per 5000 cm^{-1} interval. Generally the size of the basis used in an MCDF calculation determines the number of energy levels that can be constructed, each approximation a solution of the many-electron Dirac equation. However, due to numerical uncertainties, not all of these energy levels have a physical meaning. Especially those that consist only of basis elements constructed from weakly bound single-electron orbitals are numerically unstable. Fortunately such energy levels are collected at energies close to the ionization threshold. This can be checked by observing the convergence of the level density at different energy ranges. While the level density converges and is stable for the energy range under consideration in the present work, an increasing number of non-physical energy levels can be observed at higher energies.

With this setup we achieve a good convergence of the calculated level density, however, it has to be noted that the accuracy of our level energies does not go beyond the chosen 5000 cm^{-1} energy interval. In Fig. 4 we show a comparison of the number of known electronic levels from the database of Ref. [3], our investigations (including Ref. [4]) and the MCDF calculations for even parity levels with $J = 1/2$ to $7/2$. The calculated level density shows a qualitative agreement with the measurements apart from a prevailing shift to higher energies. The most apparent feature of the level density plot is the minimum around 60000 cm^{-1} . The existence of this minimum comes with an experimental uncertainty, because it lies on the border of the covered energy range of both

measurements. Our calculations, however, reproduce this qualitative behaviour, confirming the experimental findings.

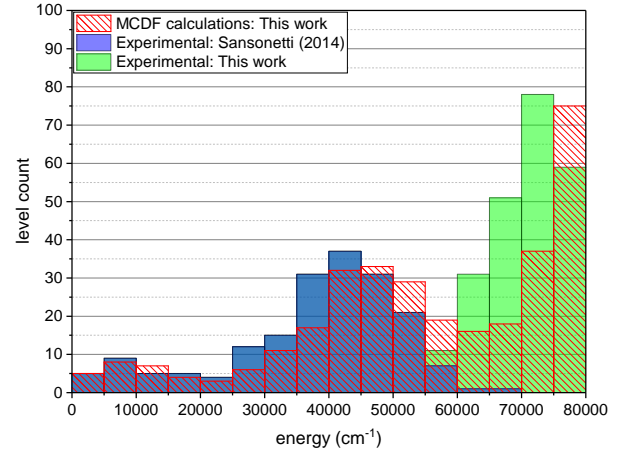


FIG. 4. Histogram of the number of electronic levels in Th^+ with $J = 1/2$ to $7/2$ and even parity in the energy range up to 80000 cm^{-1} . The calculated level numbers are shown in red, the measured level numbers in blue (Ref. [3]) and green (this work).

Based on our calculations and the experimental findings we can estimate the enhancement factor β for the excitation of the ^{229}Th nuclear transition via an electronic bridge process [10]. Following Ref. [16] we find the average energy interval between two levels in the desired energy range between 60000 cm^{-1} and 65000 cm^{-1} to be $160 \text{ cm}^{-1} < D_p < 280 \text{ cm}^{-1}$. Assuming that the electronic bridge starts from the $J_i = 3/2$ ground state of Th^+ via an even parity intermediate level with angular momentum in the range $1/2 < J_n < 7/2$, and with the present value and uncertainty for the nuclear transition frequency ω_N , we get: $0.5 \times 10^3 < \beta < 6 \times 10^3$. However this value strongly depends on ω_N and increases rapidly for $\omega_N > 70000 \text{ cm}^{-1}$. A similar result has recently been obtained for the electronic bridge decay rate in Th^+ [13].

VI. CONCLUSION

We have measured the energies of 166 previously unknown high-lying levels in the energy range from 7.8 to 9.8 eV in $^{232}\text{Th}^+$ and have determined the angular momenta of many of the newly found levels, as well as for previously unclassified levels reported in Ref. [4]. We furthermore have performed MCDF calculations which allow us to predict the electronic level density with acceptable accuracy in the investigated energy range.

The good agreement between measured and calculated level density gives rise to the assumption that most of the even-parity levels with $J = 1/2$ to $7/2$ in the energy range from 7.8 to 9.8 eV were found.

The resonant excitation of the nuclear isomer through high-lying levels in $^{229}\text{Th}^+$ is expected to be enhanced compared to the direct optical excitation [8–10, 22]. In comparison to the investigated energy range in the previous experiment [4] and ab-initio calculations [16, 23],

the level density measured in this work is significantly higher. Therefore we can expect an increased excitation probability for the nuclear isomer via these newly found high-lying levels.

ACKNOWLEDGMENTS

We thank O. A. Herrera-Sancho and K. Zimmermann for contributions to the experimental setup and S. Klein for assistance in the experiment. We furthermore thank T. Leder, M. Menzel, B. Lipphardt and A. Hoppmann for providing expert technical support. We acknowledge financial support from the European Union's Horizon 2020 Research and Innovation Programme under Grant Agreement No. 664732 (nuClock) and from DFG through CRC 1227 (DQ-mat, project B04).

Appendix A: Excitation pathways and angular momentum determination of high-lying levels

TABLE III: Newly observed high-lying states excited through the intermediate levels listed in Tab. I together with levels observed in our previous experiment [4] (marked with "*"). The symbol "x" marks levels which are successfully excited via the specified intermediate level and the symbol "—" denotes that no excitation is observed. If no symbol is given, the excitation has not been checked. Where possible, the levels are given with their total angular momenta derived from the experiment. The energy of the level marked with ** from Ref. [4] is updated. Levels with angular momentum $J = 3/2$ are classified unambiguously.

Level [cm ⁻¹]	Intermediate levels															J_{exp}
	J = 1/2					J = 3/2					J = 5/2					
	a	b	c	d	e	f	g	h	i	j	k	l	m	n	o	
58875.5	*	-								x						3/2 - 7/2
59387.1	*	-								x						3/2 - 7/2
59477.4	*	x								x						3/2
59803.0	*	-								x						3/2 - 7/2
60380.1	*	x								x						3/2
60618.6	*	x								x						3/2
60721.3	*	-								x						3/2 - 7/2
61032.4	*	x				x				x						3/2
61388.0	*	-				-				x						3/2 - 7/2
61428.6	*	-				x				x						3/2 or 5/2
61726.3	*	x	x			x	x			x						3/2
61963.6	*	x	x			x	x			x						3/2
62307.2	*	-				x	x			x						3/2 or 5/2
62373.8	*	x	x			x	x			x	x					3/2
62477.0	*	-				x	x			x	x					3/2 or 5/2
62560.1	*	-				-	-			x	x					3/2 or 5/2
62562.2	*	x	x			x	x			x	x					3/2
62753.1	*	-				x	x			x	x					3/2 or 5/2
62873.11		x				x	x			-	-					1/2 or 3/2
63257.5	*	-				-	-			x	x					3/2 - 7/2
63268.90	x	x				x	x			-	-					1/2 or 3/2
63298.4	*	-				-	-			x	x					3/2 - 7/2
63557.7	*	-				-	-			x	x					3/2 - 7/2
63680.29	x	x				x	x			x	x					3/2
64107.51	-	-				x	x			x	x					3/2 or 5/2
64122.0	*	-				-	-			x	x					3/2 - 7/2
64150.3	*	x	x			x	-			x	x					3/2
64368.24	-	-				x	x			x	x					3/2 or 5/2
64442.11	x	x				x	x			-	-					1/2 or 3/2
64560.4	*	x	x			x	x			x	x					3/2
64813.7	*	-				-	-			x	x					3/2 - 7/2
64860.4	*	-				x	x			x	x					3/2 or 5/2
64887.80	x	x				x	x			-	-					1/2 or 3/2
64920.1	*	-				x	x			x	x					3/2 or 5/2
65037.7	*	x	x			x	x			x	x					3/2
65144.4	*	-				x	x			x	x					3/2 or 5/2
65191.1	*	-				-	-			x	x					3/2 - 7/2
65730.4	*	x	x			-	x			x	x					3/2
65738.54	**	-				-	-			x	x					3/2 - 7/2
65753.45	x	x				x	x			-	-					1/2 or 3/2
65799.6	*	x	x			x	x			x	x					3/2
65910.0	*	-				-	-			x	x					3/2 - 7/2
65946.9	*	-				-	-			x	x					3/2 - 7/2
66052.0	*	-				-	x			x	x					3/2 or 5/2
66141.2	*	-				x	x			x	x					3/2 or 5/2
66324.52	x	x				x	x			-	-					1/2 or 3/2
66333.7	*	x	x			-	x			x	x					3/2
66388.81	x	x				x	x			-	-					1/2 or 3/2
66429.64	-	-				x	x			-	x					3/2 or 5/2
66558.0	*	-				-	-			x	x					3/2 - 7/2
66609.0	*	-				x	x			x	x					3/2 or 5/2
66666.96	x	x				-	x			-	-					1/2 or 3/2

Level [cm ⁻¹]	Intermediate levels												J_{exp}		
	$J = 1/2$					$J = 3/2$				$J = 5/2$					
	a	b	c	d	e	f	g	h	i	j	k	l	m	n	o
66702.9	*	x	x		x	x	x	x			x	x			3/2
66831.1	*	x	x		x	x	x	x			x	x			3/2
66855.6	*	-		x	x	x	x			3/2 or 5/2					
67066.2	*	-		-	-	x	x			3/2 - 7/2					
67154.05	x	-		x	x		x	x			3/2				
67177.76	-	-	-	-	-	x	x			3/2 - 7/2					
67378.61	-	-	-	-	-	x	x			3/2 - 7/2					
67509.63	x		x	x		x	x				3/2				
67577.71	-	x	-		-	x				3/2 or 5/2					
67657.30	x		x	x		-	-			1/2 or 3/2					
67737.62	-		x	x		x	x			3/2 or 5/2					
67803.24	-	x	-		-	x				3/2 or 5/2					
67843.31	-	x	x		-	x				3/2 or 5/2					
67866.10	-	-	x		x	x				3/2 or 5/2					
68033.33	-	-	-	x	x					3/2 - 7/2					
68088.03	x		x	x		-	x				3/2				
68278.65	-	-	-	x	x					3/2 - 7/2					
68497.88	-	-	x		-	x				3/2 or 5/2					
68564.19	-	x	x		-	x				3/2 or 5/2					
68598.83	-	x	x		-	x				3/2 or 5/2					
68752.06	x		x	x			x				3/2				
68812.64	-		x	x		x				3/2 or 5/2					
68898.67	x		x	x			x			3/2 or 5/2					
68921.30	-	x		-	x					3/2 or 5/2					
69582.93	x			x			x				3/2				
70036.57	x			x			x				3/2				
70602.32		x			x			x			3/2 or 5/2				
70618.40		x			x			x			3/2 or 5/2				
70747.82		-	-		x	x					3/2 - 7/2				
70924.75	-	x			x			x			3/2 or 5/2				
71038.37	x	-	x		x			x			3/2				
71043.67	-	-	-	x	x					3/2 - 7/2					
71148.96	-	x		x		x				3/2 or 5/2					
71153.87	x		x	x		x					3/2				
71278.32	x		x	x		-				1/2 or 3/2					
71309.24	-	x		x		x				3/2 or 5/2					
71345.59	x		x	x		-				1/2 or 3/2					
71457.82	-	-	-	x	x					3/2 - 7/2					
71543.05	x		x	x		x					3/2				
71544.12	x		x	x		-				1/2 or 3/2					
71595.39	-	x	x	x		-				1/2 - 5/2					
71648.63	-	x	x	x		-				1/2 - 5/2					
71682.08	x		x	x		-				1/2 or 3/2					
71704.43	-	x		x		x				3/2 or 5/2					
71893.76	x		x	x		x					3/2				
71980.22	-	x		x		x				3/2 or 5/2					
71995.47	-	-	-	x	x					3/2 - 7/2					
72027.87	x		x	x		x					3/2				
72070.57	x		x	x		-				1/2 or 3/2					
72183.47	-	x		x		x				3/2 or 5/2					
72195.77	-	x		x		x				3/2 or 5/2					
72353.67	-	-	-	x	x					3/2 - 7/2					
72395.99	-	x		x		x				3/2 or 5/2					
72403.45	x		x	x		x					3/2				
72437.78	x		x	x		-				1/2 or 3/2					
72443.68	-	x		x		x				3/2 or 5/2					
72612.99	-	x		x		x				3/2 or 5/2					
72624.83	x		x	x		x					3/2				
72644.97	-	-	-	x	x					3/2 - 7/2					
72711.86	-	-	-	x	x					3/2 - 7/2					
72748.31	x		x	x		x					3/2				
72756.38	-	-	-	x	x					3/2 - 7/2					
72849.84	x		x	x		x					3/2				
72904.32	-	-	-	x	x					3/2 - 7/2					
72937.01	-	x		x		x				3/2 or 5/2					
72967.30	x		x	x		x					3/2				
73007.80	x		x	x		-				1/2 or 3/2					
73141.86		x			x						x				3/2
73171.82		-			-	-				x	x				3/2 - 7/2
73225.52		x			x						x				3/2
73245.52		-			x						x				3/2 or 5/2
73314.63		-			-	-				x	x				3/2 - 7/2
73349.33		x			x						-				1/2 or 3/2
73427.59		x			x						x				3/2
73486.18		-			x						x				3/2 or 5/2
73506.20		x			x						-				1/2 or 3/2
73514.42		-			-	-				x	x				3/2 - 7/2
73571.40		-			x						x				3/2 or 5/2
73637.54		-			x						x				3/2 or 5/2
73717.33		x			x						x				3/2
73720.66		-			-	-				x	x				3/2 - 7/2
73856.76		-			x						x				3/2 or 5/2
73927.39		-			x						x				3/2 or 5/2
74015.17		-			-	-				x	x				3/2 - 7/2
74035.55		x			x						x				3/2
74041.31		-			-	-				x	x				3/2 - 7/2
74077.59		-			x						x				1/2 - 5/2
74159.76		-			x						x				3/2 or 5/2
74195.13		-			x						x				3/2 - 7/2
74201.68		x			x						x				1/2 or 3/2
74255.11		-			x						x				3/2 or 5/2
74328.90		-			x						x				3/2 or 5/2
74396.40		-			x						x				3/2 or 5/2
74461.06		-			-	-				x	x				3/2 - 7/2
74503.38		-			x					x	x				3/2 or 5/2
74554.39		x			x					x	x				3/2
74642.51		-			x					x	x				3/2 or 5/2
74646.94		x			x					x	x				1/2 or 3/2
74781.76		-			x					x	x				3/2 or 5/2
74823.59		-			x					x	x				3/2 or 5/2
74881.76		x			x					x	x				3/2
75009.01		-			x					x	x				3/2 or 5/2
75058.06		-			x					x	x				3/2 - 7/2
75108.36		-			x					x	x				3/2 or 5/2
75129.42		-			x					x	x				1/2 - 5/2
75172.74		-			x					x	x				3/2 or 5/2
75324.44		-			x					x	x				3/2 - 7/2
75380.56		-			x					x	x				3/2 or 5/2
75434.83		-			x					x	x				3/2 - 7/2
75553.70		x			x					x	x				1/2 or 3/2
75568.80		-			x					x	x				3/2 or 5/2
75613.54		x			x					x	x				3/2
75690.72		x			x					x	x				1/2 or 3/2
75783.69		-			x					x	x				3/2 or 5/2
75840.96		-			x					x	x				3/2 or 5/2
75889.36		x			x					x	x			</	

Level [cm ⁻¹]	Intermediate levels										<i>J_{exp}</i>			
	J = 1/2	J = 3/2	J = 5/2	J = 7/2	J = 9/2	J = 11/2	J = 13/2	J = 15/2	J = 17/2	J = 19/2				
a	b	c	d	e	f	g	h	i	j	k	l	m	n	o
77154.88	-	x	x	-	-	-	-	-	-	-	-	-	-	-
77185.31	-	-	-	-	x	x	3/2 - 7/2	-	-	-	-	-	-	-
77208.86	-	-	x	-	-	x	3/2 or 5/2	-	-	-	-	-	3/2 - 7/2	-
77278.24	x	-	x	-	-	-	1/2 or 3/2	-	-	-	-	-	1/2 or 3/2	-
77295.28	-	-	x	-	-	x	3/2 or 5/2	-	-	-	-	-	1/2 or 3/2	-
77311.25	x	-	x	-	-	x	3/2	-	-	-	-	-	1/2 or 3/2	-
77429.20	x	-	x	-	-	-	1/2 or 3/2	-	-	-	-	-	1/2 or 3/2	-
77506.72	-	-	x	x	-	-	1/2 - 5/2	-	-	-	-	-	1/2 or 3/2	-
77668.89	-	-	x	-	-	x	3/2 or 5/2	-	-	-	-	-	1/2 or 3/2	-
77715.95	x	x	-	-	-	-	1/2 or 3/2	-	-	-	-	-	1/2 or 3/2	-
77914.52	x	-	x	-	-	-	1/2 or 3/2	-	-	-	-	-	1/2 or 3/2	-
77992.06	-	-	-	-	x	x	3/2 - 7/2	-	-	-	-	-	1/2 or 3/2	-
78004.65	x	-	x	-	-	x	3/2	-	-	-	-	-	1/2 or 3/2	-

Appendix B: List of newly observed lines

TABLE IV: Vacuum wavelengths λ and their uncertainties σ of the newly found lines in $^{232}\text{Th}^+$ between electronic levels in the energy range from 7.8 to 9.8 eV. The classification shows the initial and final level with energy in cm⁻¹.

λ [nm]	σ [pm]	Classification	λ [nm]	σ [pm]	Classification	λ [nm]	σ [pm]	Classification
237.3774	0.5	25027 – 67154	252.6039	0.6	36582 – 76169	269.2348	0.6	26965 – 64108
237.3854	0.6	26626 – 68752	252.6795	0.5	36391 – 75966	269.4283	0.6	36391 – 73506
238.4730	0.5	26965 – 68899	252.7839	0.6	28244 – 67803	269.5733	0.6	36391 – 73486
238.5148	0.5	37130 – 79056	252.9017	0.6	36582 – 76123	269.7499	0.5	37130 – 74202
238.9628	0.6	26965 – 68813	253.1719	0.5	36391 – 75889	269.8782	0.6	26626 – 63680
239.2760	0.6	28244 – 70037	253.2042	0.9	28244 – 67738	269.9864	0.5	27403 – 64442
239.3099	1.5	26965 – 68752	253.3508	0.6	36688 – 76159	270.0000	0.6	36391 – 73428
239.8737	0.5	36391 – 78079	253.3928	0.9	26965 – 66430	270.0321	0.8	36688 – 73721
239.9382	0.5	36688 – 78365	253.4829	0.6	36391 – 75841	270.0562	0.5	36688 – 73717
240.0962	0.5	37130 – 78780	253.4919	0.6	37846 – 77295	270.5256	0.7	27403 – 64368
240.1541	0.6	25027 – 66667	253.6557	0.7	26965 – 66389	270.5716	0.7	36391 – 73349
240.1903	0.6	26965 – 68599	253.6645	0.6	37130 – 76552	270.6395	0.5	36688 – 73638
240.2932	0.5	37130 – 78746	253.7101	0.5	25027 – 64442	270.9641	0.5	37130 – 74036
240.3025	0.6	36391 – 78005	253.8512	0.6	36391 – 75784	271.1246	0.6	36688 – 73571
240.3337	1.2	26424 – 68033	254.0696	0.7	26965 – 66324	271.3337	0.5	36391 – 73246
240.3905	0.7	26965 – 68564	254.1993	0.5	37846 – 77185	271.4550	0.6	35157 – 71995
240.7252	0.5	37130 – 78671	254.2338	0.9	28244 – 67578	271.4809	0.5	36391 – 73226
240.8251	0.5	36391 – 77914	254.3518	0.5	37130 – 76446	271.5441	0.5	36688 – 73514
240.8585	0.6	27403 – 68921	254.3619	0.7	26424 – 65739	271.7525	0.9	36688 – 73486
240.8879	0.5	37130 – 78643	254.4261	0.6	35157 – 74461	272.0991	0.5	36391 – 73142
240.9901	0.6	27403 – 68899	254.4506	1.0	36391 – 75691	272.1860	0.8	36688 – 73428
241.1881	0.6	26626 – 68088	254.5932	0.5	36688 – 75966	272.3679	0.5	26965 – 63680
241.1969	0.5	36688 – 78148	254.6741	0.5	28244 – 67510	272.4475	0.6	27403 – 64108
241.3031	0.7	26424 – 67866	254.6875	0.6	27403 – 66667	272.9075	0.7	26626 – 63269
241.4906	0.6	27403 – 68813	254.6952	0.6	36688 – 75951	273.0251	0.7	36688 – 73315
241.5974	0.4	36688 – 78079	254.8353	0.5	37130 – 76371	273.0951	0.5	36391 – 73008
241.7691	0.5	25027 – 66389	254.9522	0.8	36391 – 75614	273.3214	0.6	37130 – 73717
241.8040	0.5	37130 – 78486	255.2435	0.5	36391 – 75569	273.3974	0.5	36391 – 72967
241.8445	0.5	27403 – 68752	255.3419	0.5	36391 – 75554	273.5413	0.6	36688 – 73246
241.8936	0.8	37716 – 79057	255.4066	0.6	37846 – 76999	273.6242	0.7	36391 – 72937
241.9013	0.6	28244 – 69583	255.4080	0.5	36688 – 75841	273.6915	0.8	36688 – 73225
242.0322	0.7	36688 – 78005	255.5270	0.6	28244 – 67379	274.0937	0.5	36688 – 73172
242.0537	1.3	26424 – 67738	255.5784	0.6	26626 – 65753	274.2783	0.5	36391 – 72850
242.1069	0.5	36688 – 77992	255.7825	0.7	36688 – 75784	274.3188	0.9	36688 – 73142
242.1455	0.6	25027 – 66325	256.1596	2.1	35157 – 74195	274.9072	0.5	37130 – 73506
242.2577	0.5	36391 – 77669	256.2301	0.5	37130 – 76158	275.0443	0.5	36391 – 72748
242.3828	0.7	26586 – 67843	256.2361	0.6	27403 – 66430	275.4539	0.8	26965 – 63269
242.5118	0.6	37130 – 78365	256.4610	0.5	37130 – 76123	275.4751	0.7	35157 – 71458
242.7445	0.9	27403 – 68599	256.4758	0.5	36391 – 75381	275.5027	0.5	37130 – 73428
242.8248	0.6	37130 – 78312	256.5036	0.7	27403 – 66389	275.6395	0.6	36688 – 72967
242.9481	0.6	27403 – 68564	256.8454	0.6	28244 – 67178	275.6561	0.7	27403 – 63680
243.1749	1.6	26965 – 68088	256.9013	0.6	36688 – 75613	275.8693	0.6	36688 – 72937
243.2133	0.5	36391 – 77507	256.9285	0.8	27403 – 66325	275.8881	0.6	26626 – 62873
243.3403	0.6	27403 – 68498	257.0019	0.8	28244 – 67154	275.9814	0.5	36391 – 72625
243.3971	0.6	26424 – 67510	257.1727	0.5	35157 – 74041	276.0718	0.5	36391 – 72613
243.5233	0.8	37716 – 78780	257.1963	0.6	36688 – 75569	276.0983	0.7	37130 – 73349
243.6726	0.5	36391 – 77429	257.4926	0.5	37130 – 75966	276.1184	0.5	36688 – 72904
243.7195	0.9	26626 – 67657	257.8103	0.6	26965 – 65753	276.4793	0.6	37846 – 74015

TABLE IV: Cont.: Newly found lines in $^{232}\text{Th}^+$.

λ [nm]	σ [pm]	Classification	λ [nm]	σ [pm]	Classification	λ [nm]	σ [pm]	Classification
243.7263	0.4	37716 – 78746	257.8501	0.7	36391 – 75173	276.5345	0.6	36688 – 72850
244.0161	0.6	36688 – 77669	257.9293	0.6	37846 – 76616	276.8210	0.6	28244 – 64368
244.0454	0.5	37130 – 78106	258.0047	0.6	37130 – 75889	277.0452	0.8	37130 – 73226
244.1713	0.5	37716 – 78671	258.0855	0.5	36688 – 75435	277.2511	0.5	36688 – 72756
244.1757	1.8	26424 – 67379	258.1385	0.5	36391 – 75129	277.3133	0.6	36688 – 72748
244.3369	0.7	37716 – 78643	258.2791	0.7	36391 – 75108	277.3683	0.7	36391 – 72444
244.3483	0.5	36582 – 77507	258.4474	0.6	36688 – 75381	277.4136	0.5	36391 – 72438
244.3746	0.4	36391 – 77311	258.6471	0.6	37846 – 76509	277.5932	0.7	36688 – 72712
244.4703	0.5	36391 – 77295	258.7102	0.9	25027 – 63680	277.6781	0.6	36391 – 72403
244.5992	0.7	26626 – 67510	258.8228	0.5	36688 – 75324	277.6888	0.5	37130 – 73142
244.6299	0.6	26965 – 67843	258.9434	0.9	36391 – 75009	277.7356	0.6	36391 – 72396
244.6534	0.5	37130 – 78004	259.3105	0.8	35157 – 73721	278.1098	0.6	36688 – 72645
244.7108	0.7	24874 – 65739	259.3339	0.6	37130 – 75691	278.2661	0.6	36688 – 72625
244.8703	0.5	26965 – 67803	259.4178	0.7	36582 – 75129	278.3578	1.2	36688 – 72613
244.9879	0.4	36391 – 77209	259.7993	0.6	36391 – 74882	278.4901	0.5	26965 – 62873
245.1924	0.4	37130 – 77915	259.8435	1.0	36688 – 75173	278.6548	0.4	35157 – 71044
245.2641	0.6	26965 – 67738	259.8534	0.6	37130 – 75614	278.7266	0.5	37130 – 73008
245.2809	0.7	37716 – 78486	260.1927	0.6	36391 – 74824	278.8179	0.7	27403 – 63269
245.3122	0.5	36391 – 77155	260.2582	0.7	37130 – 75554	278.8335	0.6	28244 – 64108
245.3790	0.6	26424 – 67178	260.2784	0.5	36688 – 75108	279.0227	0.7	35199 – 71038
245.5220	0.7	26424 – 67154	260.4762	0.7	36391 – 74782	279.0418	0.7	37130 – 72967
245.5409	0.5	25027 – 65753	260.6201	0.5	36688 – 75058	279.2888	0.6	36391 – 72196
245.7206	0.4	36582 – 77278	260.7055	0.8	35157 – 73514	279.3846	0.5	36391 – 72183
245.7479	0.5	26965 – 67657	260.7547	0.6	27403 – 65753	279.6758	0.5	36688 – 72444
245.7913	0.6	27403 – 68088	260.9534	0.6	36688 – 75009	279.9593	0.5	37130 – 72850
245.8277	0.5	36391 – 77069	261.0119	0.5	37846 – 76159	279.9907	0.5	36688 – 72403
245.8363	0.5	28244 – 68921	261.3606	0.5	26626 – 64888	280.0492	0.9	36688 – 72396
245.9731	0.6	28244 – 68899	261.3941	0.6	36391 – 74647	280.2686	0.6	36391 – 72071
246.1642	0.6	36688 – 77311	261.4244	0.5	36391 – 74642	280.3815	0.5	36688 – 72354
246.2293	0.8	26965 – 67578	261.4936	1.0	25027 – 63269	280.6046	0.5	36391 – 72028
246.3333	0.5	37716 – 78312	261.8229	0.7	36688 – 74882	280.7571	0.5	37130 – 72748
246.3919	0.6	37130 – 77716	261.8774	0.6	28244 – 66430	280.9699	0.5	35157 – 70748
246.4680	0.6	36582 – 77155	262.0282	0.5	36391 – 74554	280.9798	1.5	36391 – 71980
246.4951	0.9	28244 – 68813	262.0705	0.5	35157 – 73315	281.6281	0.6	36688 – 72196
246.5258	0.5	36391 – 76954	262.2221	0.4	36688 – 74824	281.6646	0.6	36391 – 71894
246.6431	0.6	26965 – 67510	262.3787	0.6	36391 – 74503	281.7263	0.6	36688 – 72183
246.7863	0.6	36688 – 77209	262.4378	0.5	37846 – 75950	281.7341	0.5	37130 – 72625
246.8632	0.7	28244 – 68752	262.5101	0.5	36688 – 74782	281.9289	0.7	27403 – 62873
246.8845	0.7	36391 – 76895	263.0554	0.6	35157 – 73172	282.1953	0.5	28244 – 63680
246.9300	0.5	36688 – 77185	263.1173	0.6	36391 – 74396	282.9669	0.6	36688 – 72028
247.1398	0.7	27403 – 67866	263.4730	0.6	36688 – 74643	283.1745	0.6	36391 – 71704
247.2790	0.6	27403 – 67843	263.5480	0.6	26424 – 64368	283.2260	0.5	36688 – 71995
247.5877	0.5	37716 – 78106	263.5858	0.7	36391 – 74329	283.2265	0.5	37130 – 72438
247.6388	0.6	36688 – 77069	263.6953	0.6	26965 – 64888	283.3486	0.5	36688 – 71980
247.8005	0.6	28244 – 68599	264.0863	0.5	36688 – 74554	283.3539	0.5	36391 – 71682
247.9269	0.7	27403 – 67738	264.0991	0.6	36391 – 74255	283.5023	0.7	37130 – 72403
248.0138	0.9	28244 – 68564	264.4414	0.6	26626 – 64442	283.6226	0.6	36391 – 71649
248.0668	0.5	36688 – 77000	264.4425	0.9	36688 – 74503	284.0444	0.5	36688 – 71894
248.1285	0.6	37846 – 78148	264.4723	0.5	36391 – 74202	284.0516	0.6	36391 – 71595
248.1460	0.5	37130 – 77429	264.7389	0.7	36688 – 74461	284.4657	0.7	36391 – 71544
248.3469	0.6	36688 – 76954	264.7654	0.5	36391 – 74160	284.4745	0.7	36391 – 71543
248.4217	0.7	27403 – 67657	264.7791	0.6	37846 – 75614	285.1681	0.5	36582 – 71649
248.4222	0.6	28244 – 68498	264.8908	0.6	37130 – 74882	285.5804	0.5	36688 – 71704
248.7104	0.6	36688 – 76895	264.9191	0.5	35157 – 72904	285.6014	0.6	36582 – 71595
248.7107	0.4	36582 – 76789	265.1928	0.4	36688 – 74396	286.0816	0.5	36391 – 71346
248.8253	0.6	26965 – 67154	265.3429	0.5	36391 – 74078	286.2032	0.5	37130 – 72071
248.8755	0.6	37130 – 77311	265.3714	0.7	26424 – 64108	286.3793	0.5	36391 – 71309
248.9909	0.8	36391 – 76553	265.6399	0.7	36391 – 74035	286.5529	0.5	37130 – 72028
249.0787	0.6	37130 – 77278	265.6679	0.5	36688 – 74329	286.6332	0.5	36391 – 71278
249.0916	0.5	37846 – 77992	265.9613	0.8	35157 – 72756	286.9024	0.5	36688 – 71543
249.1837	0.5	36391 – 76522	266.0379	0.6	37846 – 75435	287.0462	0.6	35199 – 70037
249.3359	0.6	27403 – 67510	266.1902	0.5	36688 – 74255	287.6058	0.5	36688 – 71458
249.7475	0.7	26626 – 66667	266.2772	0.5	35157 – 72712	287.6587	0.5	37130 – 71894
250.0034	0.6	37716 – 77716	266.4047	0.6	36391 – 73927	287.6592	0.6	36391 – 71154
250.1207	0.8	36391 – 76371	266.5487	0.5	37130 – 74647	287.7000	0.5	36391 – 71149
250.4481	0.5	36688 – 76616	266.6159	0.5	36688 – 74195	288.6182	0.5	36391 – 71038
250.8486	0.5	36688 – 76553	266.6953	0.6	36582 – 74078	288.8402	0.5	36688 – 71309
250.8504	0.5	36582 – 76446	266.7042	0.9	28244 – 65739	289.4210	0.5	37130 – 71682

TABLE IV: Cont.: Newly found lines in $^{232}\text{Th}^+$.

λ [nm]	σ [pm]	Classification	λ [nm]	σ [pm]	Classification	λ [nm]	σ [pm]	Classification
250.8733	0.5	25027 – 64888	266.7522	0.5	35157 – 72645	289.5678	0.5	36391 – 70925
250.9774	0.6	28244 – 68088	266.7761	0.6	27403 – 64888	290.1422	0.5	36688 – 71154
251.0241	0.5	36391 – 76227	266.8226	1.1	37846 – 75324	290.1833	0.5	36688 – 71149
251.0444	0.5	36688 – 76522	266.8315	0.6	26965 – 64442	290.5814	0.5	37130 – 71544
251.1051	0.5	37130 – 76954	266.8689	0.6	36688 – 74160	290.5905	0.5	37130 – 71543
251.1249	0.6	36688 – 76509	266.9070	0.6	36391 – 73857	290.8340	0.6	35199 – 69583
251.3195	0.4	36582 – 76372	267.2075	0.5	37130 – 74554	291.0724	0.5	36688 – 71044
251.3223	0.8	28244 – 68033	267.3579	0.9	26965 – 64368	291.1177	0.6	36688 – 71038
251.3902	0.5	36391 – 76169	267.7137	0.5	36688 – 74041	292.0836	0.5	36688 – 70925
251.4636	0.5	36391 – 76158	267.7552	0.7	36688 – 74036	292.1596	0.5	36391 – 70618
251.4767	0.5	37130 – 76895	267.9015	0.5	36688 – 74015	292.2673	0.5	37130 – 71346
251.4936	0.6	26626 – 66389	267.9039	0.5	36391 – 73717	292.2969	0.6	36391 – 70602
251.5668	0.7	27403 – 67154	268.4147	0.6	26424 – 63680	292.8431	0.5	37130 – 71278
251.6860	1.0	36391 – 76123	268.4778	0.6	36391 – 73638	293.6014	0.5	36688 – 70748
251.9026	0.8	26626 – 66324	268.5331	0.7	36688 – 73927	293.9144	0.5	37130 – 71154
252.1521	0.5	37130 – 76789	268.7301	0.7	37846 – 75058	294.7209	0.5	36688 – 70618
252.2345	0.8	36582 – 76227	268.8409	0.6	35157 – 72354	294.8605	0.5	36688 – 70602
252.3841	0.8	28244 – 67866	268.9555	0.6	36391 – 73571			
252.5284	0.7	28244 – 67843	269.0431	0.5	36688 – 73857			

- [1] E. F. Worden, J. Blaise, M. Fred, N. Trautmann, and J.-F. Wyart, in: *The Chemistry of the Actinide and Transactinide Elements, chap. 16*, 3rd ed., edited by L. R. Morss, N. Edelstein, J. Fuger, and J. J. Katz, Vol. 3 (Springer Netherlands, 2006).
- [2] C. Lovis and F. Pepe, *Astron. Astrophys.* **468**, 1115 (2007).
- [3] S. L. Redman, G. Nave, and C. J. Sansonetti, *Astrophys. J. Suppl. Ser.* **211**, 4 (2014).
- [4] O.A. Herrera-Sancho, N. Nemitz, M.V. Okhapkin, and E. Peik, *Phys. Rev. A* **88**, 012512 (2013).
- [5] N. Rosenzweig and C. E. Porter, *Phys. Rev.* **120**, 1698 (1960).
- [6] B. Beck, J. Becker, P. Beiersdorfer, G. Brown, K. J. Moody, J. B. Wilhelmy, F. Porter, C. Kilbourne, and R. Kelley, *Phys. Rev. Lett.* **98**, 142501 (2007).
- [7] B. R. Beck, G. V. Brown, R. L. Kelley, J. A. Becker, C. Y. Wu, F. S. Porter, J. B. Wilhelmy, C. A. Kilbourne, J. K. Moody, *et al.*, LLNL-PROC-415170 (2009).
- [8] E. V. Tkalya, V. O. Varlamov, V. V. Lomonosov, and S. A. Nikulin, *Phys. Scripta* **53**, 296 (1996).
- [9] F. Karpeshin, I. Band, and M. Trzhaskovskaya, *Nucl. Phys. A* **654**, 579 (1999).
- [10] S. G. Porsev, V. V. Flambaum, E. Peik, and C. Tamm, *Phys. Rev. Lett.* **105**, 182501 (2010).
- [11] E. Peik and M. Okhapkin, *C. R. Phys.* **16**, 516 (2015).
- [12] B. Seiferle, L. von der Wense, and P. G. Thirolf, *Phys. Rev. Lett.* **118**, 042501 (2017).
- [13] F. F. Karpeshin and M. B. Trzhaskovskaya, *Nucl. Phys. A* **969**, 173 (2018)
- [14] R. Zalubas and C. H. Corliss, *J. Res. Natl. Bur. Stand. Sect. A* **78A**, 163 (1974).
- [15] M. V. Okhapkin, D. M. Meier, E. Peik, M. S. Safranova, M. G. Kozlov, and S. G. Porsev, *Phys. Rev. A* **92**, 020503 (2015).
- [16] V. A. Dzuba and V.V. Flambaum, *Phys. Rev. Lett.* **104**, 213002 (2010).
- [17] O.-A. Herrera-Sancho, *Laser excitation of 8-eV electronic states in Th^+ : A first pillar of the electronic bridge toward excitation of the Th-229 nucleus*, Ph.D. thesis, Leibniz Universität Hannover (2012).
- [18] O. A. Herrera-Sancho, M. V. Okhapkin, K. Zimmermann, C. Tamm, E. Peik, A. V. Taichenachev, V. I. Yudin, and P. Głowacki, *Phys. Rev. A* **85**, 033402 (2012).
- [19] P. Jónsson, G. Gaigalas, J. Bieron, C. F. Fischer, and I. Grant, *Comp. Phys. Commun.* **184**, 2197 (2013).
- [20] C. Froese-Fischer and T. Brage, *Computational atomic structure: an MCHF approach* (CRC Press, 1997).
- [21] I. P. Grant, *Relativistic Quantum Theory of Atoms and Molecules: Theory and Computation*, 1st ed., Springer Series on Atomic, Optical, and Plasma Physics, Vol. 40 (Springer-Verlag New York, 2007).
- [22] F. Karpeshin, I. Band, M. Trzhaskovskaya, and M. Listengarten, *Phys. Lett. B* **372**, 1 (1996).
- [23] S. G. Porsev and V. V. Flambaum, *Phys. Rev. A* **81**, 032504 (2010)